ISSN 1070-3632, Russian Journal of General Chemistry, 2022, Vol. 92, No. 4, pp. 611–628. © Pleiades Publishing, Ltd., 2022.
Russian Text © The Author(s), 2022, published in Zhurnal Obshchei Khimii, 2022, Vol. 92, No. 4, pp. 578–597.

To the 90th Anniversary of the Birth of A.I. Rusanov

Stability of Metastable Phases and Kinetics of Nucleation in a Simple Single-Component System (Molecular Dynamics Simulation) (A Review)

V. G. Baidakov[a,*]

[a] *Institute of Thermal Physics, Ural Branch of the Russian Academy of Sciences, Yekaterinburg, 620016 Russia*
**e-mail: baidakov@itpuran.ru*

Received February 15, 2022; revised February 15, 2022; accepted March 15, 2022

Abstract—The review presents the results of molecular dynamics simulation of metastable states in the systems of the Lennard–Jones particles. The boundaries of the existence of metastable phases of liquid, gas, and crystal and their coexistence on a flat separating surface have been discussed. The data on the kinetics of fluctuation formation of a new phase in a superheated and supercooled liquid as well as in a superheated crystal have been analyzed within the framework of the classical nucleation theory. Peculiarities in the behavior of stability of the metastable phases have been established. The material is largely based on the works of the author and his colleagues.

Keywords: metastable state, molecular dynamics, classical nucleation theory, spinodal, binodal

DOI: 10.1134/S107036322204003X

1. INTRODUCTION

First-order phase transitions in a system of many particles and the possibility of coexistence of the phases in equilibrium are among the manifestation of the intermolecular interactions. Disturbance of equilibrium between the coexisting phases is due to relative decrease in stability of one of them, the internal stability with respect to small disturbance of the state parameters being retained. It seems as if a single phase does not exhibit any sensitive indicator of the transition across the line of the equilibrium with another phase. This allows the intrusion of a phase into the field of existence of another one, where the former phase is metastable.

It has been suggested that the region of a metastable phase existence is restricted, and at certain supersaturation it loses the property to reduce the infinitely small disturbances, i.e. becomes absolutely unstable. This boundary is known as the boundary of the phase significant instability or the spinodal.

A phase equilibrium line divides the thermodynamic surface of the uniform system into the regions of stable and metastable states and is the boundary of the absolute stability of the phase [1].

Breakup of a metastable system starts with the fluctuation appearance of small inclusions (nuclei) with the properties of the competing phase. The nucleation is related to the passing through the energy barrier, the height of which determined the work to form the critical nucleus, the smallest stable formation of a novel phase.

The nuclei evolution can be described by the classical nucleation theory based on fundamental physical principles [2, 3]. In this sense, the theory is universally applicable to liquid, gaseous, and crystalline phases. The critical nuclei are regarded as macroscopic objects in the theory.

Experimental studies of metastable phases have been limited by relatively low supersaturation [4–8], which is due to the impossibility of complete removal of the foreign (heterogeneous) inclusions in the system as well as its finite lifespan.

Computer modeling methods, primarily the molecular dynamics approach [9, 10] have opened new possibilitirs to investigate the phase metastability. Small size of the molecular dynamics models and ensured "purity" of the system allow deep penetration into the metastable regions which are still unavailable in a natural experiment.

This review demonstrates the results of the molecular dynamics modeling of metastable states of liquid, gas, and crystal un the systems containing a limited number of particles, the interaction between which can be described using the Lennard–Jones pairwise additive potential [11]

$$u_{LJ}(r) = 4\varepsilon\left[\left(\frac{\sigma}{r}\right)^{12} - \left(\frac{\sigma}{r}\right)^{6}\right], \qquad (1)$$

with r being the interparticle distance; ε and σ being the parameters characterizing the energy of dispersive interaction between the particles and their size. Along with the Boltzmann's constant k_B and the particles mass m, the σ and ε parameters are used to reduce the values obtained via the molecular dynamics modeling to the dimensionless scale. Hereafter, the values are given in the dimensionless scale, unless stated otherwise. For argon, $\sigma = 0.3405$ nm, $\varepsilon/k_B = 119.8$ K, and $m = 6.6336\times10^{-26}$ kg.

2. STABILITY OF METASTABLE PHASES

Figure 1 displays the phase diagram of a single-component Lennard–Jones system in the pressure–temperature and temperature–density coordinates. Parameters of the critical point of the Lennard–Jones system are: $T_c = 1.332$, $p_c = 0.1371$, and $\rho_c = 0.3111$; these of the triple point are: $T_t = 0.692$, $p_t = 0.0012$, $\rho_{t,l} = 0.847$, and $\rho_{t,g} = 0.0018$ [12].

Thermodynamics determines the boundary of the significant instability of the metastable phase (the spinodal) via the following conditions [1, 4]:

$$-\left(\frac{\partial p}{\partial \upsilon}\right)_T = \left(\upsilon\beta_T\right)^{-1} = 0, -\left(\frac{\partial T}{\partial s}\right)_p = \frac{T}{C_p} = 0. \qquad (2)$$

with $\upsilon = 1/\rho$ being specific volume, β_T being isothermal compressibility, s being entropy, C_p being heat capacity at constant pressure. Let us consider the boundaries of significant instability of the metastable phases in the Lennard–Jones system.

Superheated (stretched) liquid and supersaturated vapor. Depth of the penetration in the metastable region and, hence, the range of the states at which the thermodynamic parameters can be obtained by means of molecular dynamics modeling is restricted by spontaneous nucleation, the boundary of the accessible supersaturation (see below). Therefore, determination of the spinodal is always related to extrapolation of the stability coefficients in condition (2) beyond this boundary. The calculation of the p, ρ, and T parameters of the Lennard–Jones fluid has revealed that the isochores of the liquid and gas in the stable as well as metastable regions are close to straight lines in the p, T plane [13]. This fact has simplified elaboration of the equation of state common of the stable and metastable phases, which, according to conditions (2) has afforded the spinodal.

Spinodal is the envelope of isochores in the p, T coordinates [4]. This property of the isochores, in view of their closeness to straight lines, has allowed the use of graphical method to determine the spinodal position.

Spinodals of the superheated (stretched) liquid *CF* and the supersaturated vapor *CD* meet in the critical point, where they have a common tangent (critical isochore) in the p, T plane (Fig. 1). At $T < 1.18$, the liquid spinodal is located at the range of negative pressure. For the spinodal and binodal, the straight diameter rule is approximately held in the T, ρ coordinates: half-sum of densities of the liquid and vapor for isothermal conditions is a linear function of temperature.

The fluctuations of density and energy are strong about the spinodal. According to thermodynamic theory of stability [4], whereas the superheated liquid and supersaturated vapor at the spinodal lose the reductive reaction with respect to infinitely small isothermal disturbance of density and energy, they are stable with respect to adiabatic changes in the parameters of state. The results of molecular dynamics modeling [12] have confirmed the finite values of adiabatic compressibility

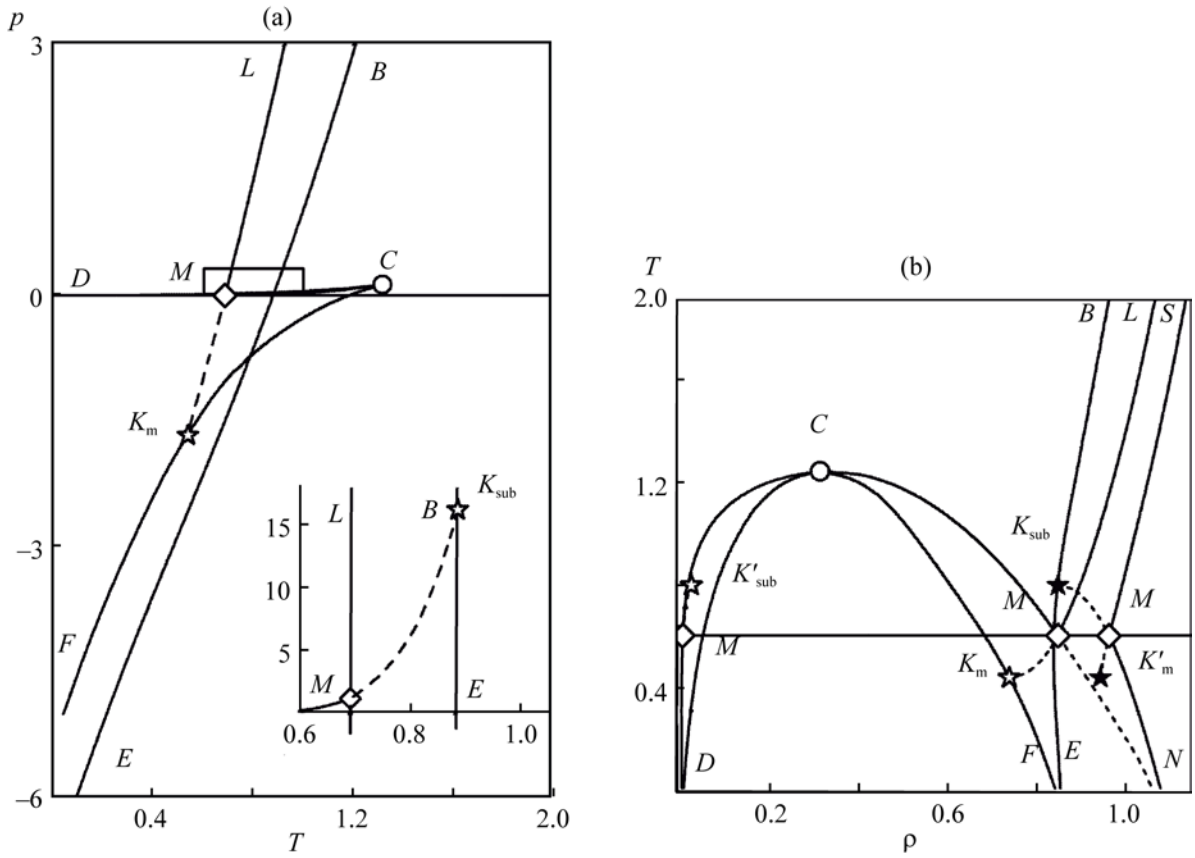

Fig. 1. Projections of the p, T (a) and T, ρ (b) phase equilibriums lines and their metastable continuations (dashed lines). Spinodals of the superheated crystal BE, stretched liquid CF, and supersaturated vapor CD; C is the critical point; K_m is the endpoint of the metastable continuation of the melting line; K_{sub} is the endpoint of the metastable continuation of the sublimation line; M is the triple point.

$\beta_s = (\partial\upsilon/\partial p)_s/\upsilon$ and isochoric heat capacity $C_\upsilon = T(\partial s/\partial T)_\upsilon$ at the spinodals of liquid and gas.

The loss of mechanical stability in a two-component liquid–vapor system is preceded by the development of diffusion instability [14]. The latter phenomenon means that the infinitely small disturbances of the solution concentration are enhanced by the reaction of the system itself. Taking the molar fraction of one of the components of the solution x as independent parameter, the boundary of the diffusion instability (diffusion spinodal) can be defined by the following condition:

$$\left(\frac{\partial\Delta\eta}{\partial x}\right)_{p,T} = 0, \qquad (3)$$

where $\Delta\eta = \eta_2 - \eta_1$ is the difference between the chemical potentials of the mixture component.

Mechanical spinodal of a two-component system, the line at which $(\partial p/\partial\upsilon)_{T,x} = 0$, is "embedded" into the diffusion spinodal and, in a general case, does not have common points with it. In the $x\to0$ and $x\to1$ limits, the diffusion and the mechanical spinodal meet. As in the case of a single-component system spinodal, diffusion spinodal of a binary solution exhibits the envelope property [15]. The diffusion spinodal in the p, T plane is the envelope of the set of isochores and adiabats extended into the metastable region, at $\Delta\eta$ = const. Mechanical spinodal of the solution also has a return point, but it is not identical to the critical point.

Supercooled liquid. Any first-order phase transition presumes the existence of metastable states. However, the presence of the spinodal is not a consequence of the phase metastability. Simulation of the p, ρ, T properties of a Lennard–Jones liquid about the liquid–crystal phase transition has evidenced [12] that the isothermal compressibility of the liquid is decreased (rather than increased) when approaching the melting line and penetration in the region of the supercooled states. This

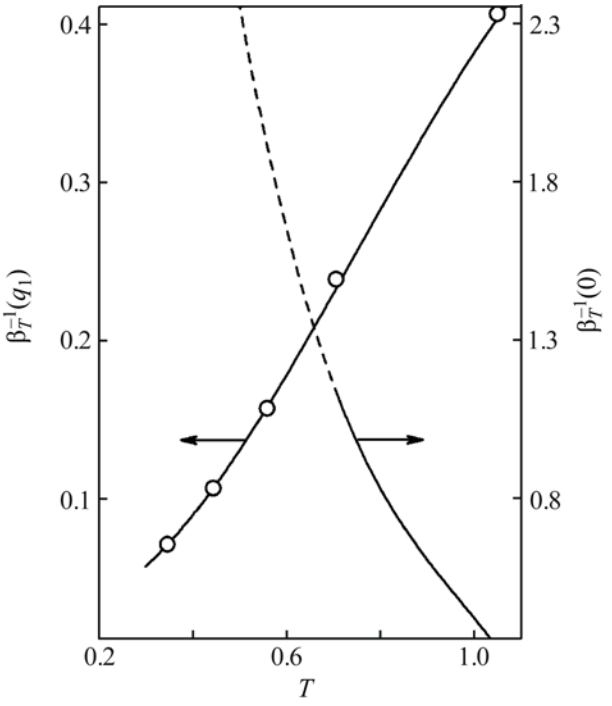

Fig. 2. Long-wave $\beta_T^{-1}(0)$ and short-wave $\beta_T^{-1}(q_1)$ elasticity of supercooled liquid.

fact evidences the increase in the liquid thermodynamic stability. Analysis of the behavior of the liquid isochores in the *p*, *T* plane about the liquid–crystal phase transition [16] has revealed that their metastable extensions do not form a convergent bundle of curves. The envelope of such shape of the υ = const lines cannot exist, i. e. the boundary determined by conditions (2), thermodynamic spinodal, is absent in the case of a single-component supercooled liquid. The absence of the spinodal of the supercooled liquid can be related to the fundamental reason of the absence of the critical point of the liquid–crystal phase equilibrium and the impossibility of continuous transition between them [17].

It has been suggested [18] that the supercooled liquid is unstable with respect to the density disturbance with the wavelength about the intermolecular distance rather than relatively long-wave thermodynamic density disturbance, i. e. local reordering of the particles is enough for the formation of a regular structure from an irregular one. The authors have estimated the temperature of the loss of stability of supercooled liquid argon at atmospheric pressure as of 64 K (0.534 dimensionless units).

The condition of mechanical stability of an isotropic phase with respect to the disturbance of an arbitrary wavelength $\lambda = 2\pi/q$ (q being the wavenumber) is as follows [19]:

$$\beta_T^{-1}(q) = \frac{\rho k_B T}{S(q)} > 0. \quad (4)$$

Here $\beta_T^{-1}(q)$ is the short-wave elasticity and $S(q)$ is the statistical structure factor.

Decrease in the liquid temperature has been accompanied by the enhancement of the first peak in the structure factor $S(q=q_1)$, evidencing the increase in the intensity of the fluctuations with the wavelength on the order of the intermolecular distance [20]. Hence, in contrast to the thermodynamic (long-wave) elasticity of the liquid $\beta_T^{-1} = \beta_T^{-1}(0)$, which is increased with the approach to the melting point and penetration in the region of the supercooled states, the short-wave elasticity $\beta_T^{-1}(q_1)$ is reduced (Fig. 2).

Reaction of the system on the time-depending impacts is determined by the dynamics of its collective modes. If the change in the thermodynamic state is accompanied by excitation the frequency of which is decreased (soft mode), this fact can evidence the system approaching the boundary of the dynamic stability.

To elucidate such boundary in the supercooled Lennard–Jones liquid via molecular dynamics modeling, the dynamic structure factor $S(q,\omega)$ has been calculated [20]. It has been stated that isobaric ($p = 0$) cooling of the liquid is accompanied by the decrease in the half-width of the quasi-elastic peak $S(q_1,\omega)$ (frequency of the collective mode Γ_{q1}). The Γ_{q1} frequency has been nonzero up to the temperature of $T = 0.555$ [the lowest temperature, at which the $S(q_1,\omega)$ can be calculated]. The Γ_{q1} values obtained from the $S(q_1)$ data under the Pathak–Singwi approximation [21] have been in good agreement with these found from $S(q_1,\omega)$.

Many supercooled liquids can be vitrified at low temperature. The vitrification is accompanied by the increase in the relaxation time and should lead to the equally strong decrease in the half-width of the quasi-elastic peak $S(q_1,\omega)$, in comparison with the continuous transition of the liquid phase into the crystal ordering [18].

Superheated crystal. A characteristic feature of a solid body distinguishing it from an isotropic medium is the presence of elastic shear stresses, in addition to the

bulk ones [22]. This determines the fact that solid bodies behave differently in response to infinitely small uniform and nonuniform density disturbances, and the boundaries of significant instability of a crystal with respect to each of these disturbances can be discussed. Hierarchy of phenomenological criteria of stability of superheated (stretched) crystalline phase has been introduced in a series of studies (let us mention just few of them [23–25]).

Explicit expression of the conditions of the crystal stability depends on its symmetry. The state of a cubic crystal under the action of hydrostatic pressure is stable with respect to relatively uniform deformations if the following conditions are met [26]:

$$\begin{aligned} K_T &= \left(\tilde{c}_{11} + 2\tilde{c}_{12}\right)/3 > 0; \\ \mu' &= \left(\tilde{c}_{11} - \tilde{c}_{12}\right)/2 > 0; \\ \mu &= \tilde{c}_{44} > 0. \end{aligned} \tag{5}$$

Here K_T is the isothermal all-round compression modulus, μ, μ′ are the simple and tetragonal shear moduli, $\tilde{c}_{11}$, $\tilde{c}_{12}$, $\tilde{c}_{44}$ are the effective elastic constants which are functions of temperature and pressure.

The boundary of significant instability of the crystal is determined by the first elasticity modulus to become zero. Violation of the first criterion in Eq. (5), related to the bulk deformation, is usually referred to as the spinodal instability. At μ = 0, the crystal loses its stability due to simple shear along one of the symmetry directions at constant volume. The third type of instability (at μ′ = 0) is known as the Born instability. An isotropic elastic solid body is stable if $K > 0$, $\mu > 0$ [22].

Deformations and stresses in a solid state which are induced by heat motion are usually nonuniform. Spatially uniform and nonuniform density fluctuations are determined by different elasticity moduli: the all-round compression modulus K_T in the case of uniform deformations and the uniaxial compression modulus $\tilde{K}_T$ (depending on the deformation direction) in the case of nonuniform deformation.

For principal directions of the face-centered cubic (fcc) crystal lattice [27]:

$$\begin{aligned} \tilde{K}_T[100] &= K_T + 4\frac{\mu'}{3}; \\ \tilde{K}_T[110] &= K_T + 4\frac{\mu'}{3} + \mu, \\ \tilde{K}_T[111] &= K_T + \frac{\mu}{3}. \end{aligned} \tag{6}$$

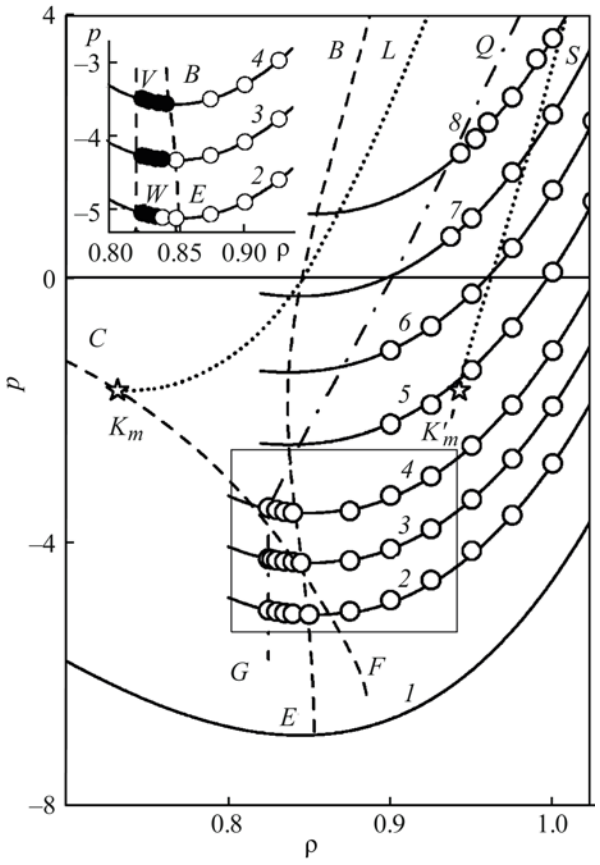

Fig. 3. Melting isotherms of an fcc crystal at T 0 (*1*), 0.2 (*2*), 0.3 (*3*), 0.4 (*4*), 0.55 (*5*), 0.7 (*6*), 0.85 (*7*), 1.0 (*8*). LK_m and SK'_m are the branches of the melting line; spinodals of the stretched liquid *CF* and the crystal *BE*; *QG* is the boundary of the limiting stretching of the crystal; *VW* is the boundary of significant instability with respect to the nonuniform deformations, determined by the $\tilde{K}_T[100] = 0$ condition; K_m is the endpoint of the melting line.

Hence, the spatially nonuniform density fluctuations are finite in an anisotropic crystal at the long-wave limit at $K_T = 0$, when $\mu > 0$ and $\mu' > 0$.

In the case of an isotropic solid bode, nonuniform density changes are independent of the deformation direction and are determined by the uniaxial compression modulus

$$\tilde{K}_T = K_T + \frac{4}{3}\langle\mu\rangle, \tag{7}$$

where ‹μ› is the shear modulus of the isotropic body.

Figure 3 displays the results of the pressure computation in the Lennard–Jones fcc crystal along the isotherms [28]. The last point at each isotherm corresponds to the density

below which the lifespan of the metastable crystal has not already been sufficient to determine the pressure.

At temperatures $T \leq 0.55$, the spinodal states with zero K_T modulus have been achieved. The crystal has retained its stability also at density below the spinodal value.

The results of the molecular dynamics simulation of the p, ρ, T properties of the crystal have been approximated by the local equation of state [12]. At $T \leq 0.7$, the density at the spinodal have been practically independent of temperature. The elasticity moduli of an fcc crystal determined from the effective elastic constants have shown that at low temperatures ($T \leq 0.55$) and negative pressures the instability with respect to relatively uniform bulk deformations $K_T = 0$ appears the first, whereas the Born instability [24] related to the tetragonal shear ($\mu' = 0$) is manifested at low temperatures.

The $\tilde{K}_T$[100] modulus has been the first of these for three principal directions of the Lennard–Jones fcc crystal to become zero. At $T \leq 0.55$, this occurs beyond the spinodal (due to the finite value of the μ′ modulus at the spinodal).

Metastable phase equilibriums. Thermodynamics forbids equilibrium coexistence of the stable and metastable phases at flat interphase boundary, but coexistence of two metastable phases is not forbidden. The latter fact means that each of the phase equilibrium lines (binodals) of a single-component system can be extended beyond the triple point, where the coexisting phases are metastable. The metastable extension of the melting line of ice has been observed in the experiment up to pressure of –24 MPa [29]. Surface tension at the interface between the supercooled liquid and the supersaturated vapor has been measured far from the triple point [30]. As in the case of an individual metastable phase, the issue of the limits of existence of metastable phase equilibriums appears. According to one of the scenarios, the melting line in the $T \to 0$ limit can freely reach the zero isotherm [31]. According to another scenario discussed using GaSb as the example [32] and in the single-component plasma model [33], the melting line ends at the spinodal of the liquid phase.

Metastable extension of the saturation line has been tracked to temperature $T = 0.55$ during the molecular dynamics modeling [34]. This is 0.142 dimensionless units below the triple point temperature. Penetration beyond the triple point in the melting and sublimation lines has been significantly smaller. This fact has been due to the special features of the considered model and the computational method [35]. Relatively free motion of the crystalline phase particles in the direction normal to the interphase boundary and the impossibility of the crystal lattice deformation along the interphase boundary plane lead to the appearance of stretching deformations which eliminate the phase metastability and do not allow deep penetration of such two-phase system beyond the triple point.

Direct calculation of the chemical potential (free energy) using the molecular dynamics method is impossible. However, p, ρ, and T, the internal energy parameters, can be readily determined via the modeling. Approximation of these data via thermal and calorimetric equations of state allows calculation of the chemical potentials of the coexisting phases and elucidation of the binodal parameters far from the triple point.

The results of calculation of metastable extensions of the liquid–crystal (MK_m) and crystal–gas (MK_{sub}) phase equilibrium lines are shown in Fig. 1 as dashed lines. In the negative pressure region, the metastable extension of the melting line ends at the spinodal of the stretched liquid. The sublimation line ends at the spinodal of the superheated crystal. Their intersection is at relatively low pressure and is not seen in Fig. 1 (the inset presents the enlarged corresponding part of the diagram).

Spinodal is a distinguished line in the thermodynamic surface of states, and the intersection of the metastable extension of the phase equilibrium line with the spinodal should be a distinguished point as well. At this point, if the phases are not identical, the $(\partial T/\partial \rho)_K = 0$ and $(\partial p/\partial \rho)_K = 0$ conditions are met only for one of the branches of the phase equilibrium line (this ending at the spinodal). At the melting line endpoint, $T_{m,K} = 0.5286$, $p_{m,K} = -1.7128$, $\rho_{m,l,K} = 0.7374$, and $\rho_{m,cr,K} = 0.9423$ [36]. At the sublimation line, $T_{sub,K} = 0.8874$, $p_{sub,K} = 0.01624$, $\rho_{sub,cr,K} = 0.8469$, and $\rho_{m,g,K} = 0.02125$ [12].

Low-temperature behavior of the saturation line is qualitatively different from that for the melting line. Due to the absence of the spinodal of the supercooled liquid, the metastable extension of the liquid–gas phase equilibrium line ends at the zero isotherm. The endpoint of the saturation line is in the stability region as well; it is the critical point. In this case, the intersection of the liquid binodal and spinodal coincides with the intersection of the gas binodal and spinodal, which results in the phases identity.

3. THERMODYNAMICS AND KINETICS OF NUCLEATION

Transformation of a metastable phase into a stable one is thermodynamically irreversible and occurs as a result of spontaneous nucleation and growth of the new phase nuclei. The nuclei with size above certain critical threshold can grow further.

The critical nucleus is in unstable equilibrium with the medium. If the nucleus is spherical, the conditions of its mechanical and material equilibrium are as follows:

$$p'_{\mathrm{K}} - p = \frac{2\gamma}{r_{\mathrm{K}}}, \tag{8}$$

$$\eta'(p'_{\mathrm{K}}, T) = \eta(p, T), \tag{9}$$

where r_{K} is the radius of the tension surface of the critical nucleus, γ is the surface tension, and η is the chemical potential. The prime values are for the nucleus. Surface tension as well as the pressure in the nucleus depend on its size.

The work of formation of the critical nucleus is

$$W_{\mathrm{K}} = \frac{1}{3}\gamma A_{\mathrm{K}} = \frac{1}{2}V_{\mathrm{K}}\left(p'_{\mathrm{K}} - p\right) = \frac{16\pi\gamma^3}{3\left(p'_{\mathrm{K}} - p\right)}. \tag{10}$$

Here $A_{\mathrm{K}} = 4\pi r_{\mathrm{K}}^2$, $V_{\mathrm{K}} = (4/3)\pi r_{\mathrm{K}}^3$ are the surface area and the volume of the nucleus.

Thermodynamics defines the work of the nuclei formation but do not describe their evolution; the latter issue is considered in the kinetic theory. Classical theory of the nucleation in the stationary case developed in a series of research [2, 3, 37, 38] determines the number of the viable nuclei formed in a unit volume of a metastable phase per unit time (the nucleation frequency) [3]

$$J = N_1 Z_{\mathrm{K}} D_{\mathrm{K}} \exp(-W_{\mathrm{K}}/k_{\mathrm{B}}T), \tag{11}$$

where N_1 is the number of particles per unit volume of the metastable phase, Z_{K} is the nonequilibrium factor, D_{K} is the diffusion coefficient of the nuclei over the size.

The nonequilibrium factor Z_{K} gives the relative excess of the transitions of the molecules from the metastable phase in the critical nucleus over the reverse transitions and is related to the curvature of the activation barrier at its top [3, 4]. The diffusion coefficient at the top of the activation barrier is determined by the rate of the change in the number of the molecules in the nucleus and the conditions at the boundary of the growing nucleus.

Methods of molecular dynamic modeling of nucleation. Molecular dynamics method opens vast possibilities in the study of nucleation. Small size of the molecular dynamics models allow deep penetration in a metastable states region and gain information on thermodynamics and kinetics unavailable in natural experiments. Moreover, elucidation of the shape, size, surface tension, and other parameters of the nuclei of a fluid as well as crystalline phase becomes possible.

The study by Alder and Wainwright [9] was the first where the transition of the ordered structure in the disordered one was observed, in the model of several tens of solid spheres. Nowadays, the emerged computation power of modern devices has enabled the molecular dynamics simulation in models consisting of billions of interacting particles [39].

Let us consider the principles of modern approaches to modeling of nucleation, which can be divided into the methods of direct modeling and the methods requiring certain additional procedures during integration of the particles motion equations. Direct methods of nucleation modeling include the methods of mean lifetime [4] and mean first-passage time [40].

The mean lifetime method is based on the registration of the time τ to observe the first stable nucleus in the system, the external conditions being constant. Since the fluctuation nucleation is a random event, this process is characterized by mean waiting time $\bar{\tau}$. The nucleation frequency is

$$J = \left(V \cdot \bar{\tau}\right)^{-1}, \tag{12}$$

where V is the system volume.

In the framework of the mean first-passage time, the time at which the nuclei with size of r_0 ($r_0 < r_{\mathrm{K}}$) grow to the size of r_1 ($r_1 > r_{\mathrm{K}}$) are determined. Besides the nucleation frequency, it is thus possible to calculate the critical nucleus size and the nonequilibrium factor. The range of the nucleation frequency which can be determined via the direct method is limited between 10^{-5} (10^{35} m^{-3} s^{-1}) and 10^{-10} (10^{30} m^{-3} s^{-1}). The latter limitation is due to the productivity of modern computers.

In the range of lower supersaturation, where $J < 10^{-6}$ (10^{31} m^{-3} s^{-1}), special modeling methods are applied.

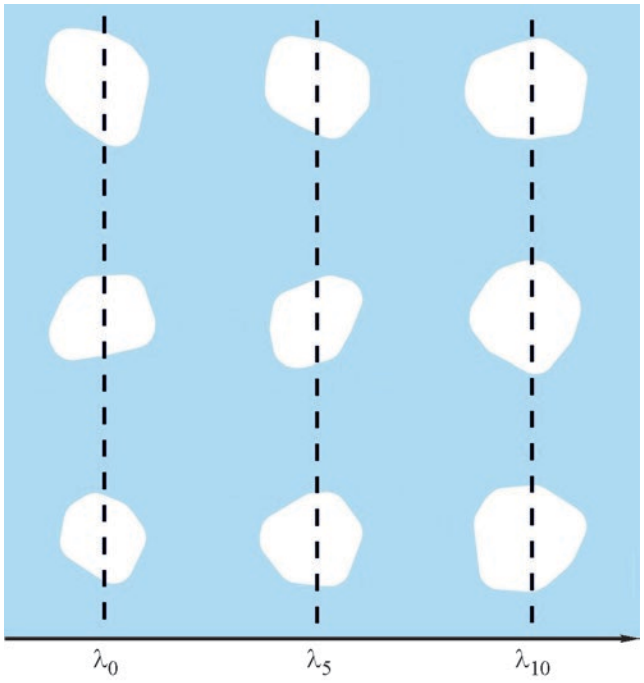

Fig. 4. Cavitation pockets in stretched liquid according to the method of sampling of transition routes in three phase surfaces at $T = 0.4$ and $p = -1.9$.

These are methods of umbrella sampling [41] and metadynamics [42], related to the introduction of the displacement potential, a function of certain collective variables, in the system Hamiltonian. The displacement potential reduces the height of the activation barrier restricting the decomposition of the metastable phase and favors the appearance of stable nuclei during shorter time as compared to direct modeling.

Another approach to accelerate the nucleation during the molecular dynamics modeling is based on the theory of transition state elaborated to compute the chemical reactions rate [43]. In this regard, let us notice the methods of checkpoints [44] and the sampling methods: these for transition routes [45], transition routes with surfaces [46]? and direct flow [47].

In the scope of the method of the transition routes sampling, phase space of the considered system is divided by several non-intersecting surfaces, each being set by the ordering parameter λ_i. The initial state is the set of points in the phase space with $\lambda \le \lambda_0$; in the final state, $\lambda \ge \lambda_n$. Frequency of the transitions from the initial into the final state, the nucleation frequency, is given by the following expression:

$$J = J_0 P(\lambda_n \mid \lambda_0), \tag{13}$$

where J_0 is the frequency of the transitions across the λ_0 surface, $P(\lambda_n|\lambda_0)$ is the probability of transitions from surface λ_0 to surface λ_n. The frequency J_0 can be computed by means of direct modeling. The probability $P(\lambda_n|\lambda_0)$ is found as the product of the probabilities of the transitions across the adjacent surfaces $P(\lambda_{i+1}|\lambda_i)$. The method of the transition routes sampling demands the introduction of special stochastic elements (ensuring fast divergence of the phase trajectories starting from the same configuration, in the procedure of integration of the particles motion equations.

A separate class of the nucleation modeling methods are these based on the introduction of an inclusion of the competing phase in the metastable one and analysis of its evolution [48, 49]. These methods are applied at low supersaturation, when the probability of appearance of other nuclei in the system is very low.

The mentioned modeling methods allow consideration of the nucleation frequency over the range of 195 orders of magnitude, from 10^{-200} and above.

Cavitation of stretched (superheated) liquid. Being metastable, a liquid can exist at negative pressure as well. Under these conditions, the critical nucleus is practically empty.

Figure 4 displays the images of cavitation pockets at three phase surfaces by means of the transition routes sampling [50]. With the increase in the cavity size, its shape approaches spherical one. At the stretching values achieved during molecular dynamics modeling, the radius of the critical pockets is of 2.3–5.1 (0.8–1.5 nm), the lower r_K value corresponding to larger stretching of the liquid phase.

Larger cavitation pockets have been investigated by means of the introduced nucleus method [50]. Up to hundred of microheterogeneous systems containing a cavity surrounded by a metastable liquid have been created in the predefined thermodynamic state. Probability of the growth of such cavities have been computed during the integration of the particles motion equations. The cavity with the growth probability of 0.5 has been considered the critical nucleus. The effective radius of the critical cavities has been of 2–12 (0.7–4.1 nm).

Using the data on the cavity radius, their surface tension has been determined from the condition of mechanical equilibrium (8). Another approach to assess γ is based on the results of the molecular dynamics modeling of the nucleation frequency (see below). The values of γ obtained by means of the mean lifetime, transition routes sampling, and nucleus introduction methods have been in good agreement between each other (Fig. 5) and coincided with the thermodynamic views on the γ(*r*) dependence [53]. Hereafter the radius of critical nucleus is assumed, although the subscript at *r* (*k*) is omitted. Within the accuracy limits, the data on γ can be approximated with the following equation:

$$\gamma(r) = \gamma_\infty \left(1 - 2\delta/r + \alpha/r^2\right), \qquad (14)$$

where the subscript ∞ relates the value to the flat surface ($r = \infty$), the parameters δ and α are functions of temperature. The expressions like (14) can be deduced from the Gibbs–Tolman equation in the limit of large *r* [54]. There, $\delta = \delta_\infty$ is the distance between the tension surface and the equimolecular dividing surface of the interfacial layer (the Tolman parameter).

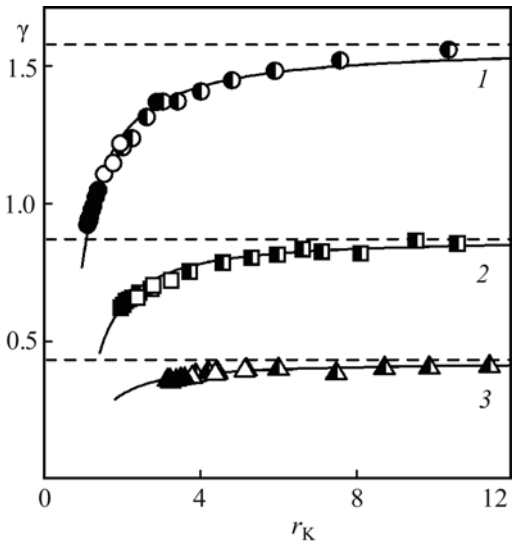

Fig. 5. Surface tension of critical bubbles in a superheated liquid at $T = 0.5$ (*1*), 0.8 (*2*), 1.0 (*3*). (Black points) mean lifetime method [51], (open points) sampling of transition routes [50], (black-white points) introduced nucleus method [50], (dashed lines) flat interphase boundary [52], (solid lines) Eq. (14).

According to the data in [50], the parameter δ in equation (14) is positive and slightly increases with the decrease in temperature. According to the data obtained by means of the Monte Carlo [55] and molecular dynamic modeling [56, 57] methods, density functional theory [55], and gradient van der Waals theory [58, 59], the value of δ_∞ in the Tolman equation is positive as well [54]. The values of δ and δ_∞ are close. The coefficient at the squared curvature of the interface calculated by means of the Monte Carlo method and the density functional theory coincides with its value in equation (14).

The work of the critical nucleus formation at the spinodal equals zero. According to equation (10), γ and r_K are zero as well. Rusanov has demonstrated [53] that at $r \to 0$ and $\gamma \to 0$, the surface tension linearly depends on the curvature radius of the tension surface of a bubble (droplet). This fact has followed from the Gibbs theory of capillarity, assuming preservation of small finite inhomogeneity at the moment of disappearance of the tension surface. When approaching the spinodal, the isothermal compressibility (and, hence, correlation radius of the fluctuations) infinitely increases. In a strongly correlated medium, the intrusion of a novel phase should possess a diffuse interphase boundary. According to Cahn and Hilliard [60], the critical inhomogeneity is marginally apparent in the vicinity of the spinodal but occupies a large region. The tension surface can be also introduced, radius of which linearly approaches zero along with the surface tension [59]. No significant increase in the diffusivity of the interphase boundary between the nucleus and the liquid has been manifested at the values of superheating (stretching) reached in the methods of mean lifetime, transition routes sampling, and incorporated nucleus.

Figure 6 displays the baric dependence of the frequency of cavitation in a stretched Lennard–Jones liquid at temperatures below ($T = 0.5$) and above ($T = 0.8$ and 1.0) that of the melting line endpoint. The algorithm of the introduced nucleus method does not allow direct computation of the nucleation frequency. However, the data on the size of cavitation pockets, diffusion coefficient, and their work of formation obtained in the framework of this method allow estimation of *J* via the equation from the classical nucleation theory (10).

The dashed lines in Fig. 6 show the results of computation of *J* using the classical nucleation theory in the macroscopic approximation, i.e. without account for the dependence of the surface tension of the

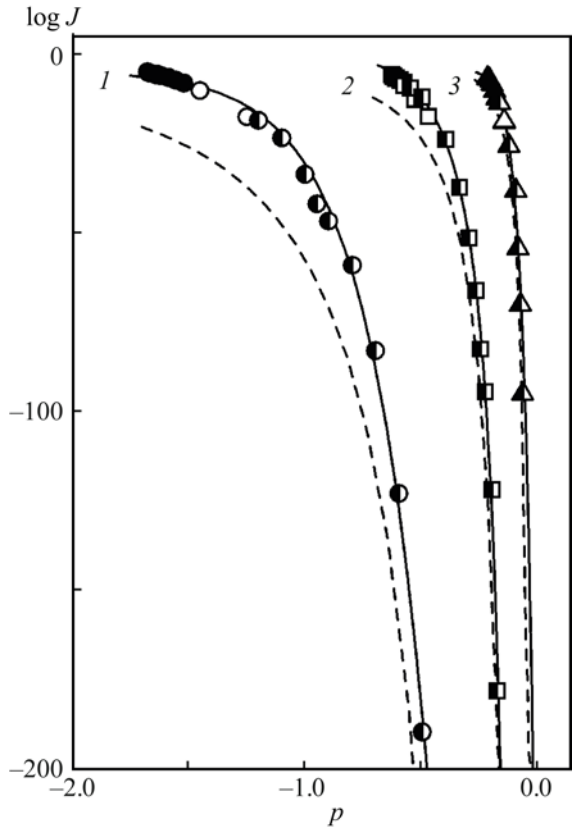

Fig. 6. Decimal logarithm of the nucleation frequency in a stretched liquid at $T = 0.5$ (*1*), 0.8 (*2*), 1.0 (*3*). (Black points) mean lifetime method [51], (open points) sampling of transition routes [50], (black-white points) introduced nucleus method [50], (dashed lines) classical nucleation theory in macroscopic approximation, (solid lines) interpolation curves.

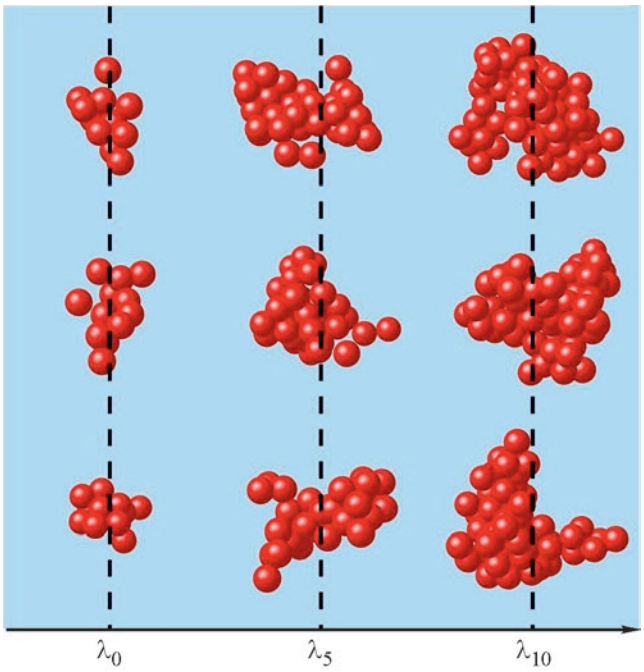

Fig. 7. Crystalline phase nuclei in a supercooled liquid according to the method of the sampling of transition routes at phase surfaces λ_0, λ_5, and λ_{10} at $T = 0.52$ and $p = 0$.

critical cavitation pocket on the interface curvature. The discrepancy between the theory and modeling data increases with the decrease in temperature and pressure. At $T = 0.5$ and $p \approx -0.5$, it is as high as 30 orders of magnitude of the nucleation frequency. Figure 5 demonstrates that this discrepancy can be due to the $\gamma(r)$ dependence.

Crystallization of supercooled (supercompressed) liquid. The images of the crystalline clusters obtained using the transition routes sampling method are shown in Fig. 7. To estimate the closeness of their shape to spherical one, tensor of the nucleus inertia has been calculated [61]. Principal radii of the central inertia ellipsoid ξ have been determined from the inertia tensor. The ratio between the largest ξ_{max} to the smallest ξ_{min} radius characterize the anisotropy of the nucleus shape. The ξ_{max}/ξ_{min} value of the crystalline nuclei in the transition routes sampling has been of 1.18–1.65 [62]. The smallest ratios have corresponded to smaller supercooling of the liquid phase.

Typical values of effective radius of the critical crystalline nuclei obtained at the supercooling achievable using the transition routes sampling [62] and umbrella sampling [63] methods have been of 2.54–3.24 (0.86–1.10 nm). The nuclei have contained 82–150 particles. Larger nuclei have been observed using the introduced nucleus method [62]. They have contained 135 to 9 000 particles, the effective radius being 3–13 (1.0–4.4 nm).

The crystal–liquid interphase boundary is characterized by mechanical and thermodynamic surface tensions, the difference between which is due to the nonuniformity of chemical potential of the static component [63, 64]. These tensions coincide for a fluid system. Hereafter we will consider certain effective surface tension in the systems with a crystalline phase.

Surface energy of the crystal nucleus is a function of crystallographic orientation of its planes, each of them exhibiting its own specific surface energy γ_i. Using the Curie–Wulff rule [49] during thermodynamic consideration of the conditions of equilibrium between a

small crystal and the supercooled liquid and introducing the effective surface tension via the spherical approximation

$$\gamma_e = \left(4\pi r_e^2\right) \int\limits_{A_e} \gamma \, dA, \qquad (15)$$

with r_e being the radius of a sphere with the volume equal to that of the equilibrium shape of the crystal with surface area A_e, it is possible to use the equations (8)–(10) for the isotropic case to calculate the wok of formation of the crystalline nucleus.

Effective surface tension at flat liquid–crystal interphase boundary $\gamma_{e,\infty}$ at temperatures above this of the melting line endpoint ($T_{m,K} = 0.529$) has been calculated in [66]. Coexistence of the metastable liquid and crystal below this temperature is impossible.

Curvature of the liquid–crystal interface (T = const) leads to the increase in the effective interface tension, which passes through a maximum and then decreases (Fig. 8). The excess of $\gamma_e(r)$ over $\gamma_{e,\infty}$ is higher at higher temperature. The $\gamma_e(r)$ dependences determined using different approaches: via the nucleation frequency (mean lifetime and transition routes sampling methods) from the data on the number of the particles in the critical nucleus and the pressure in it (transition routes sampling and introduced nucleus methods) have been in good agreement.

The $\gamma_e(r)$ dependence has been approximated using Eq. (11). At temperatures shown in Fig. 8, the δ parameter has been negative, decreasing from –0.1 to –0.38 with the decrease in temperature. The α value has been of 0.65–1.3.

Assuming than the Tolman parameter δ_∞ of the flat crystal–liquid interface is temperature-independent, it has been expressed through the excess interface values determined via molecular dynamics modeling [67]. Another approach to determine δ_∞, accounting for anisotropy of the crystal–liquid interphase boundary, has been suggested by Cheng and Ceriotti [68]. Taking advantage of metadynamics and capillary-wave model, they have calculated $\gamma_{e,\infty}$ at the equimolecular dividing surface and have determined δ_∞. At temperatures close to the triple point of the Lennard–Jones system, the δ_∞ parameter has been negative and close to 0.3–0.5 in its absolute value.

Figure 9 illustrates the results of the computation of the Gibbs number, the W_K/T ratio, in a supercooled liquid at negative, zero, and positive pressures by means

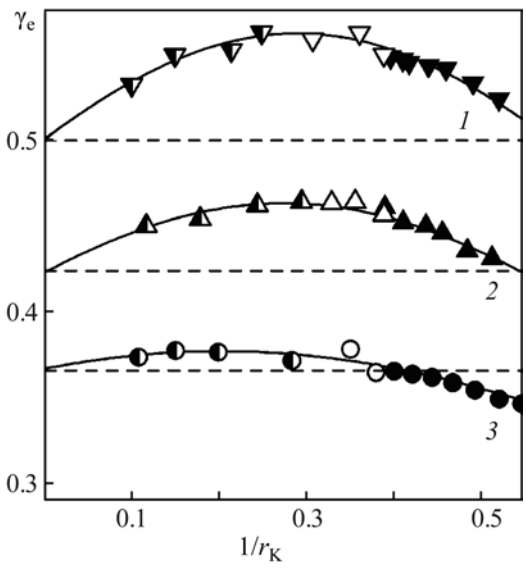

Fig. 8. Effective surface tension of critical crystalline nuclei in a supercooled liquid at T = 0.865 (*1*), 0.7 (*2*), and 0.55 (*3*). (Black points) mean lifetime method [66], (open points) sampling of transition routes [62], (black-white points) introduced nucleus method [62], (solid lines) Eq. (14), (dashed lines) flat interphase boundary [65].

of the transition routes sampling and metadynamics [69, 70]. They have been compared with the Gibbs numbers obtained using the classical nucleation theory from the molecular dynamics data on the crystallization frequency in a supercooled liquid [66].

In the framework of molecular dynamics modeling, diffusion coefficient of the crystalline nuclei can be calculated from the mean-square deviation of the number of particles in the crystalline cluster at time τ from its value in the critical nucleus

$$D_K = \frac{\left\langle \left[n(\tau) - n_K\right]^2 \right\rangle}{2\tau}. \qquad (16)$$

Here the angle brackets ‹..› denote the averaging over the ensemble. The D_K values obtained from Eq. (16) via the methods of the transition routes sampling, mean first-passage time [1, 2], and the introduced nucleus are shown in Fig. 10.

The Turnbull–Fisher equation usually used in the classical nucleation theory to determine D_K [73], assumes that the frequency of the elementary acts of the particles addition at the surface and their going away in the liquid

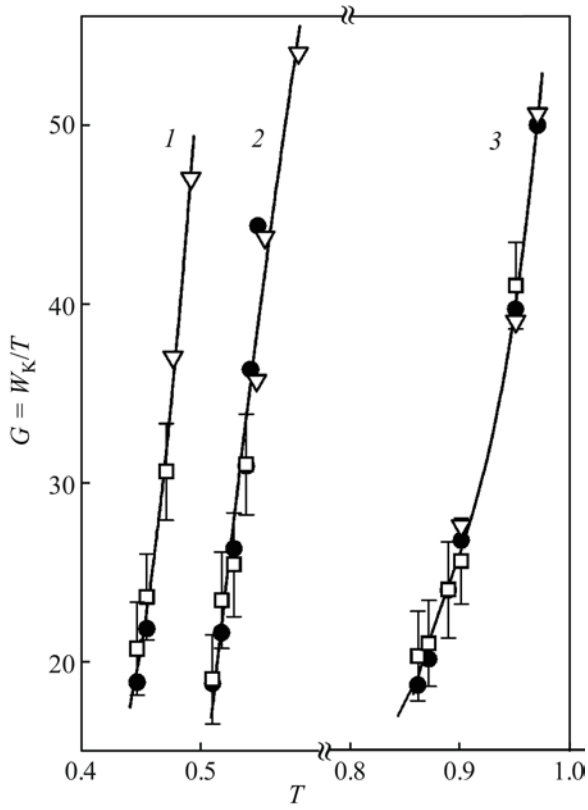

Fig. 9. Isotherms of the Gibbs number at p = –0.995 (*1*), 0 (*2*), and 6.912 (*3*). (□) metadynamics [69], (▽) sampling of transition routes [66], (●) calculation from the classical nucleation theory using the molecular dynamics data on the nucleation frequency [71].

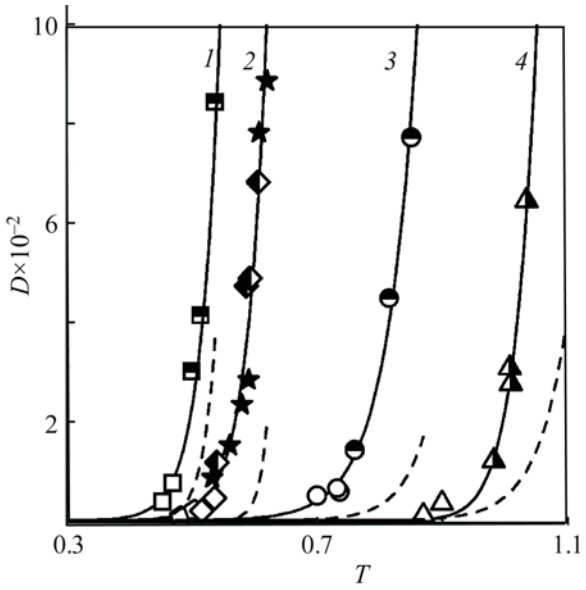

Fig. 10. Diffusion coefficient of crystalline nuclei in a supercooled liquid at p = –0.995 (*1*), 0 (*2*), 3.600 (*3*), and 6.912 (*4*). (Open points) sampling of transition routes [71], (black-white points) introduced nucleus method [71], (black points) method of mean first-passage time [72], (dashed lines) the Turnbull–Fisher equation [73], (solid lines) interpolation curves.

is the factor limiting the growth of the crystalline nucleus in the supercooled liquid. The results of calculation of D_K using the Turnbull–Fisher equation are shown in Fig. 10 in dashed lines.

Temperature dependence of the nucleation frequency for a supercooled Lennard–Jones liquid at positive and negative pressure is displayed in Fig. 11. The accuracy of determination of J is comparable to the points size in the plot. The data obtained via the mean lifetime and the transition routes sampling have been in good agreement over the range of states where both methods are applicable. The modeling results have been compared to the calculation of J using the classical nucleation theory under macroscopic approximation [66].

Nucleation in superheated (stretched) crystal. Distortion of the crystalline order in a metastable solid body can occur as a result of fluctuation appearance of a liquid phase nucleus of a cavitation pocket (crack). Deformations about the nucleus arise due to the difference in the density of the initial and the novel phases. The deformations determine the fact that the nuclei in the shape of the round lens are energetically favorable at low superheating (stretching), whereas spherical ones are favorable at high superheating [74–76].

The work of the formation of the critical spherical cavity in an isotropic elastic medium is [75]

$$W_K = \frac{16\pi\gamma_e^3}{2p^2\left[1-2p\langle\mu\rangle\Big/\left(K_T+\frac{4}{3}\langle\mu\rangle\right)^2\right]^2}, \qquad (17)$$

where ‹μ› is the shear modulus of the isotropic crystal. In contrast to the liquid, where the work of the critical nucleus formation is inversely proportional to the squared stretching, in the case of the solid body $W_K[]p^{-4}$.

The correspondence of a particle to the ordered or disordered phase during molecular dynamics modeling has been determined using the global parameter of central symmetry ψ [78]. Local parameter of the central symmetry ψ_j has been calculated for each particle in the fcc crystal [79] as

$$\psi_j = \sum_{i=1,6} \left| \vec{r}_{j,i} + \vec{r}_{j,i+6} \right|^2, \quad (18)$$

where $\vec{r}_{j,I}$ and $\vec{r}_{j,i+6}$ are the radius-vectors from particle j to two neighbor particles. The summation in equation (18) is performed over the pairs of opposite vectors for six closest pairs of particles with the lowest $|\vec{r}_{j,i} + \vec{r}_{j,i+6}|^2$ value. If the particles are fixed in the sites of ideal fcc lattice, $\psi_j = 0$. Global parameter of central symmetry can be calculated as

$$\Psi = \sum_j \psi_j / N.$$

Above the temperature of the melting line endpoint ($T_{m,K} = 0.529$), distortion of the crystalline ordering has led to the formation of the liquid phase nucleus with nearly spherical shape (Fig. 12a). The nucleus growth has been accompanied by sharp decrease in temperature and simultaneous increase in the global parameter of central symmetry (inset I) [79, 80]. Further increase in the nucleus size has not changed its shape (inset II). The nucleus was then stretched along one of the planes parallel to the unit cell planes, and a layer of liquid surrounded

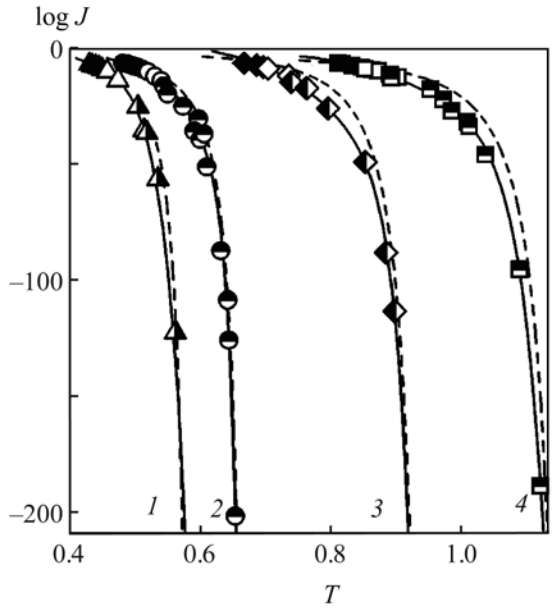

Fig. 11. Decimal logarithm of crystallization frequency of a supercooled liquid at p = 1.0 (*1*), 0 (*2*), 3.6 (*3*), and 6.912 (*4*). (Black points) mean lifetime method [66], (open points) sampling of transition routes [66], (black-white points) introduced nucleus method [66]. (Dashed lines) classical nucleation theory in macroscopic approximation [66], (solid lines) interpolation curves.

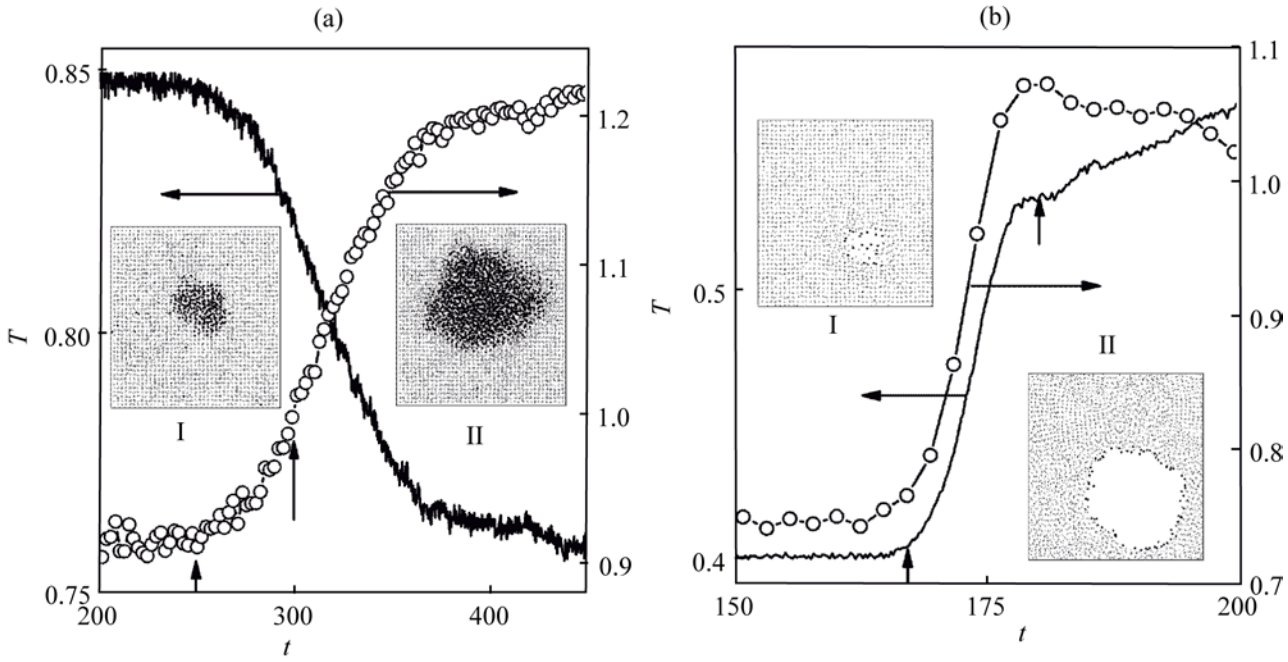

Fig. 12. Evolution of the global parameter of the central symmetry and temperature during the appearance of the liquid phase nucleus (a) (T = 0.85, ρ = 0.91) and cavity (b) (T = 0.4, ρ = 0.84) in an fcc crystal. I, II – layer of the particles with thickness 4.5 during the appearance and growth of the nucleus (the time moments are indicated with vertical arrows).

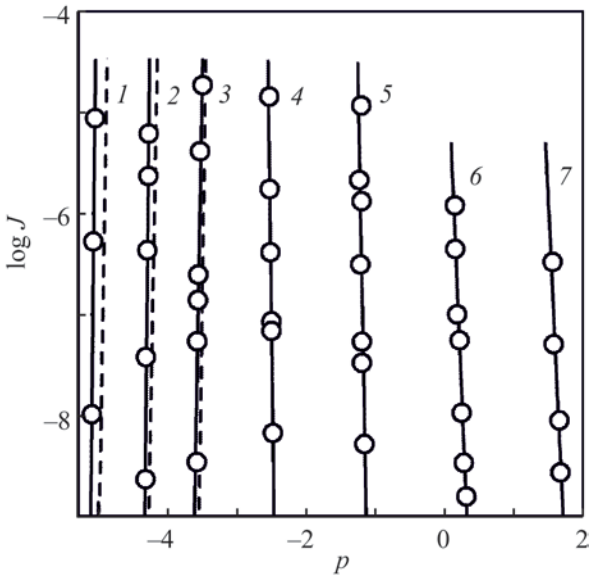

Fig. 13. Decimal logarithm of the nucleation frequency in a stretched fcc crystal at $T = 0.2$ (*1*), 0.3 (*2*), 0.4 (*3*), 0.55 (*4*), 0.7 (*5*), 0.85 (*6*), and 1.0 (*7*). (Points) mean lifetime method [80], (dashed lines) classical nucleation theory in macroscopic approximation, (solid lines) interpolation curves.

by the crystalline phase from two sides has been formed in the central part.

Another picture of the phase decay has been observed at $T < T_{m,K}$. In this case (Fig. 12b), disruption of the crystalline order has started by the appearance of a cavity (inset I) and has been accompanied by increase in the global parameter of central symmetry as well as temperature. The increase in the cavity size (inset II) has led to significant displacement of the particles from the sites of the fcc lattice. The cavity was nearly spherical in shape. The particles at its interface have exhibited enhanced mobility. The rate of the cavity growth has been about 10 times higher than the liquid droplet growth. Upon the system equilibration, the crystalline order has been restored in the surrounding phase, and the "crystal with cavity" configuration has been preserved during further modeling.

At $T = 0.55$, close to the temperature at the melting line endpoint, monotonous increase in the global parameter of central symmetry at an early stage of the phase decay of the crystal has been accompanied to the decrease in temperature, which has turned into its sharp increase. A liquid phase nucleus has appeared in the crystal, inside which a cavity has then appeared.

The described picture of the nucleation in the crystal is in line with thermodynamic considerations. The critical nucleus is in an unstable material and mechanical equilibrium with the external medium. The increase in stretching ($p_m - p$) is accompanied by the increase in the ($p_m - p_K$) difference and the decrease in r_K. At $T = 0.85$ and $p = 0.178$ ($p_m - p_K = 1.773$), the pressure in the critical nucleus has been of ≈0.35, 2.7 times higher than the pressure in the liquid–gas critical point, which has ensured stable state of the liquid phase in the nucleus.

At $T = 0.7$ and $p = -1.255$, the pressure in the critical nucleus has been lower than this at the liquid–gas phase equilibrium line but higher than the pressure at the spinodal of the stretched liquid ($p_{sp} \approx -1.0$). The liquid phase in the critical nucleus has been metastable. Below $T_{m,K}$, the equilibrium coexistence of the metastable crystal with the metastable liquid has been impossible at planar as well as curved interphase boundary [81]. In this case, the appearance of the liquid phase nucleus is ruled out, and the phase decay of the crystal occurs via the appearance and growth of the cavities (pores).

And positive and small negative pressures ($p > p_{m,K}$), the crystalline phase has lost the relaxation reaction with respect to uniform deformations until approaching the spinodal ($K_T = 0$), where the tetragonal shear modulus turns zero ($\mu' = 0$). This line is the upper boundary of the crystal superheating where spontaneous nucleation of the liquid phase is possible. The spinodal states have been reached during the molecular dynamics modeling below $p_{m,K}$, and the penetration beyond the spinodal, its value increasing with the decrease in temperature, has been observed (the inset in Fig. 3). Such behavior of the stability of the crystalline phase evidences finite value of the activation barrier W_K at the spinodal, and since the shear modulus $\langle\mu\rangle \neq 0$ at $K_T = 0$, then, according to equation (17), the effective surface tension at the crystal–cavity interface is finite (positive) as well.

The possibility of the penetration beyond the solid body spinodal at the vicinity of the tricritical point has been considered by Levanyuk [82]. The slabbing strength of iron measured using femtosecond lasers has been close to the spinodal one [83].

Figure 13 illustrates the baric dependence of the nucleation frequency in a stretched fcc crystal at temperatures above and below the melting line endpoint [80]. The data on J have been obtained using the mean lifetime method. Whereas at $T > T_{m,K}$ the nucleation frequency has increased with the decrease in density and

pressure, the increase in J at $T < T_{m,K}$ has been observed with the decrease in density and the increase in pressure. The latter phenomenon has been due to the transition beyond the spinodal.

The molecular dynamics modeling data have been compared with the results of calculation of J using classical nucleation theory (Fig. 13, dashed lines) under macroscopic approximation. The values of γ_e at the planar crystal–liquid and crystal–gas interphase boundaries have been determined in [81, 84]. Whereas the discrepancy in the values of the nucleation frequency from the molecular dynamics modeling and classical nucleation theory has been up to seven orders of magnitude ($T = 0.2$), the slopes of the isotherms of J have been close.

The effective surface tension of the critical nuclei calculated from the data on the nucleation frequency is 30–60% lower than this at the planar interphase boundary, at $T < T_{m,K}$ (the nucleus is a cavity) as well as at $T > T_{m,K}$ (the nucleus is a liquid droplet).

4. CONCLUSIONS

Experimental studies of metastable states are complicated by their finite "lifetime" and high "sensitivity" to external stimuli inducing the phase transition. The methods of molecular dynamics modeling have opened novel possibilities in the investigation of phase instability, allowing verification of theories and elucidating novel features in the behavior of partially equilibrium systems. These approaches have been illustrated in this review using the Lennard–Jones system as an example.

It has been shown that each of the phases in a single-component system is restricted by the spinodal, the boundary of thermodynamic instability, only from one side. The spinodals of liquid and crystalline phases can be reached by their heating (stretching), and this of gas is reached by cooling (compression). There is no spinodal in the case of the supercooled liquid. Retaining the relaxation properties with respect to long-wave (thermodynamic) infinitely small changes in density, the supercooled liquid loses its stability towards the disturbances with the wavelength of the intermolecular distances order.

Shear stresses in the solid body lead to its different response to infinitely small uniform and nonuniform deformations, which are determined by different elasticity moduli. The molecular dynamics modeling has shown that the tetragonal shear modulus μ' is the first to turn zero at temperatures above the temperature of the melting line endpoint $T_{m,K}$ (classical result of the Born stability theory). At the $\mu' = 0$ line, the uniaxial compassion moduli for the principal directions in the fcc crystal are positive. At $T < T_{m,K}$, the spinodal state with $K_T = 0$ and $\tilde{K}_T \neq 0$ can be reached. The boundary of the ideal strength of the fcc crystal is determined by the $\tilde{K}_T$ modulus turning zero [100].

The lines of melting, sublimation, and saturation can be extended beyond the triple point. Metastable extensions of the melting and sublimation lines end at their intersection with the spinodals of the liquid and crystal, respectively. Metastable extension of the saturation line does not have such point. The endpoint of the liquid–gas phase equilibrium ends in the stable states region. In this region, the binodals of the coexisting phases meet their spinodals, which leads to the identity of the phases and anomalous increase in the fluid susceptibility to external stimuli.

The decay of a metastable system starts with the appearance and growth of the nuclei of the novel (competing) phase. The nucleation frequency J is increased with the penetration in the metastable region. The $J = 10^6$–10^{27} m^{-3} s^{-1} range has been reached in the natural experiments [8]. The upper limit of this range is determined by the spatial-time factor, the lower limit being due to heterogeneous and induced nucleation. Molecular dynamics modeling has eliminated some of the said restrictions and extended the range of the studies. Limited number of the particles in the molecular dynamics models and short time of their evolution allow the realization of the nucleation frequency in the range of $J = 10^{30}$–10^{35} m^{-3} s^{-1}. the methods of metadynamics, transition routes sampling, and the introduced nucleus have decreased the lower limit of the range to to 10^{-160} m^{-3} s^{-1}, thus covering the range of the natural experiment and significantly extending it.

When the nucleation frequency if changed by 200 orders of magnitude, the critical nucleus radius is changed by an order of magnitude, to 0.5 nm and more. This fact has allowed observation of the formation of the stable nucleus at low supersaturations in the systems of several thousands of the interacting particles, by introduction of additional procedures in the algorithm of integration of the motion equations.

Classical nucleation theory considers the nuclei as "macroscopic" objects and describes them with the thermodynamic parameters of the macrophases. Molecular dynamics has allowed verification of this theory considering the final result (the nucleation

frequency, which is typical of the natural experiment) as well as the details (nonequilibrium factor, diffusion coefficient, and work of the critical nucleus formation). Hence, possibility of the extension of thermodynamics to such small objects as the nuclei has been demonstrated and it has been shown that the classical nucleation theory is qualitatively correct in the description of the evolution of the nuclei at small supersaturations, for which it has been elaborated, as well as at high degree of metastability.

AUTHOR INFORMATION

V.G. Baidakov, ORCID: https://orcid.org/0000-0002-7775-4914

ACKNOWLEDGMENTS

The author is grateful to the Supercomputer Center, Institute of Mathematics and Mechanics, Ural Branch of the Russian Academy of Sciences for the allocated computing time.

CONFLICT OF INTEREST

No conflict of interest was declared by the authors.

REFERENCES

1. Gibbs, J.V., *Termodinamika. Statisticheskaya mekhanika* (Thermodynamics. Statistical Mechanics), Moscow: Nauka, 1982
2. Volmer, M. and Weber, A., *Z. Physik. Chem. (A)*, 1926, vol. 119, nos. 3–4, p. 277.
3. Zel'dovich, Ya.B., *Zh. Eksp. Tekh. Fiz*., 1942, vol. 12, no. 11–12, p. 525.
4. Skripov, V.P., *Metastabil'naya zhidkost'* (Metastable Liquid), Moscow: Nauka, 1972.
5. Skripov, V.P., Sinitsyn, E.N., Pavlov, P.A., Ermakov, G.V., Muratov, G.N., and Baidakov, V.G., *Teplofizicheskie svoistva zhidkostei v metastabil'nom sostoyanii* (Thermophysical Properties of Liquids in a Metastable State), Moscow: Atomizdat, 1980.
6. Skripov V.P. and Koverda V.P., *Spontannaya kristallizatsiya pereokhlazhdennykh zhidkostei* (Spontaneous Crystallization of Supercooled Liquids), Moscow: Nauka, 1984.
7. Debenedetti, P.G., *Metastable Liquids: Concepts and Principles*, Princeton: Princeton University Press, 1996.
8. Baidakov, V.G., *Explosive Boiling of Superheated Cryogenic Liquids*, Weinheim: WILEY-VCH Verlag GmbH&Co. KGaA, 2007.
9. Alder, B.J. and Wainwright, T.E., *J. Chem. Phys*., 1959, vol. 27, p. 1208. https://doi.org/10.1063/1.1743957
10. Alder, B.J. and Wainwright, T.E., *J. Chem. Phys*., 1959, vol. 31, no. 2, p. 459. https://doi.org/10.1063/1.1730376
11. Jones, J., *Proc., R. Soc. London (A)*, 1924, vol. 106, p. 441. https://doi.org/10.1098/rspa.1924.0082
12. Baidakov, V.G. and Protsenko, S.P., *Zh. Eksp. Tekh. Fiz*, 2006, vol. 130, no. 6(12), p. 1014.
13. Baidakov, V.G. and Protsenko, S.P., *Teplofiz. Vys. Temp*., 2003, vol. 41, no. 2, p. 231.
14. Prigozhin, I. and Defei, R., *Khimicheskaya termodinamika* (Chemical Thermodynamics), Novosibirsk: Nauka, Sibirskoe Otdelenie, 1966.
15. Baidakov, V.G., *Fluid Phase Equilib*., 2018, vol. 471, p. 61. https://doi.org/10.1016/j.fluid.2018.05.001
16. Skripov, V.P. and Baidakov, V.G., *Teplofiz. Vys. Temp*., 1972, vol. 10, no. 6, p. 1226.
17. Landau, L.D. and Lifshits, E.M., *Statisticheskaya fizika* (Statistical Physics), Moscow: Nauka, 1964.
18. Schneider, T., Broui, R., Thomas, H., and Feder, J., *Phys. Rev. Lett*., 1970, vol. 25, p. 1423.
19. Schneider, T., Srinivasan, G., and Enz, C.P., *Phys. Rev. (A)*, 1972, vol. 2, p. 15281.
20. Baidakov, V.G., Galashev, A.E., and Skripov, V.P., *Fiz. Niz. Temp*., 1976, vol. 2, no. 8, p. 957.
21. Pathak, K.N. and Singwi, K.S., *Phys. Rev. (A)*, 1970, vol. 2, p. 2427.
22. Landau, L.D. and Lifshits, E.M., *Teoriya uprugosti* (Theory of Elasticity), Moscow: Nauka, 1965.
23. Lindemann, F.A., *Z. Phys*., 1910, vol. 11, p. 609.
24. Born, M., *J. Chem. Phys*., 1939, vol. 7, no. 8, p. 591.
25. Hill, R., *Math. Proc. Camb. Phil. Soc*., 1975, vol. 77, p. 225.
26. Wang, J., Li, Ju., Yip, S., Phillot, S., and Wolf, D., *Phys. Rev. (B)*, 1995, vol. 52, no. 17, p. 12627. https://doi.org/10.1103/physrevb.52.12627
27. Zhurkov, S.N. and Narzullaev, B.N., *Zh. Tekh. Fiz.*, 1953, vol. 23, no. 10, p. 1657.
28. Baidakov, V.G. and Tipeev, A.O., *Teplofiz. Vys. Temp*., 2018, vol. 56, no. 2, p. 193
29. Henderson, S.J. and Speedy, R.J., *J. Phys. Chem*., 1978, vol. 91, p. 13069.
30. Ritter, M.B., Awschalom, D.D., and Shafer, M.W., *Phys. Rev. Lett*., 1988, vol. 61, no. 8, p. 966. https://doi.org/10.1103/PhysRevLett.61.966
31. Skripov, V.P. and Faizullin, M.Z., *Teplofiz. Vys. Temp*., 1999, vol. 37, no. 5, p. 814.

32. Ponyatovskii, E.G., *Pis'ma Zh. Eksp. Tekh. Fiz*., 1997, vol. 66, no. 4, p. 260.
33. Iosilevskii, I.L. and Chigvintsev, A.Yu., *Issledovano v Rossii* (Researched in Russia), 2003. http://zhurnal.ape.relarn.ru/articles/2003/003.pdf
34. Baidakov, V.G., Chernykh, G.G., and Protsenko, S.P., *Zh. Fiz. Khim*., 2000, vol. 74, no. 8, p. 1382.
35. Baidakov, V.G. and Protsenko, S.P., *J. Eng. Thermophys*., 2007, vol. 16, no. 4, p. 249.
36. Baidakov, V.G. and Protsenko, S.P., *Phys. Rev. Lett*., 2005, vol. 95, p. 015701. https://doi.org/10.1103/PhysRevLett.95.015701
37. Doring, W., *Z. Phys. Chem*., 1936, vol. 36, p. 371.
38. Volmer, M., *Kinetik der Phasenbildung*, Dresden; Leipzig: Verlag Th. Steinkopff, 1939.
39. Diemand, J., Angélil, R., Tanaka, K.K., and Tanaka, H., *J. Chem. Phys*., 2013, vol. 139, p. 074309. https://doi.org/10.1063/1.4818639
40. Wedekind, J., Strey, R., and Requera, D., *J. Chem. Phys*., 2007, vol. 126, p. 134103. https://doi.org/10.1063/1.2713401
41. Torrie, G.M. and Valleau, J.P., *Chem. Phys. Lett*., 1974, vol. 28, no. 4, p. 578. https://doi.org/10.1016/0009-2614(74)80109-0
42. Laio, A. and Parrinello, M., *Proc. Natl. Acad. Sci. USA*, 2002, vol. 99, no. 20, p. 12562. https://doi.org/10.1073/pnas.202427399
43. Glasstone, S., Laidler, K.J., and Eyring, H., *The Theory of Rate Processes; The Kinetics of Chemical Reactions, Viscosity, Diffusion and Electrochemical Phenomena*, New York: McGeaw-Hill Book Company, 1941.
44. Faradjian, A.K. and Elber, R., *J. Chem. Phys*., 2004, vol. 120, no. 23, p. 10880. https://doi.org/10.1063/1.1738640
45. Bolhuis, P.G., Chandler, D., Dellago, C., and Geissler, P.L., *Annu. Rev. Phys. Chem*., 2002, vol. 53, p. 291. https://doi.org/10.1146/annurev.physchem.53.082301.113146
46. van Erp, T.S., Moroni, D., and Bolhuis, P.G., *J. Chem. Phys*., 2003, vol. 118, no. 17, p. 7762. https://doi.org/10.1063/1.1562614.
47. Allen, R.J., Valeriani, C., and ten Wolde, P.R., *J. Phys. Condens. Matter*., 2009, vol. 21, p. 463102. https://doi.org/10.1088/0953-8984/21/46/463102
48. Espinosa, J.R., Vega, C., Valeriani, C., and Sanz, E., *J. Chem. Phys*., 2003, vol. 144, no. 3, p. 034501. https://doi.org/10.1063/1.4939641
49. Rosales-Pelaez, P., Sanchez-Burgos, I., Valeriani, C., Vega, S., and Sanz, E., *Phys. Rev. (E)*, 2020, vol. 101, p. 022611. https://doi.org/10.1103/PhysRevE.101.022611
50. Baidakov, V.G. and Protsenko, K.R., *Chem. Phys. Lett*., 2020, vol. 760, p. 138030. https://doi.org/10.1016/j.cplett.2020.138030
51. Baidakov, V.G. and Bobrov, K.S., *J. Chem. Phys*., 2014, vol. 140, p. 184506. https://doi.org/10.1063/1.4874644
52. Baidakov, V.G., Protsenko, S.P., Kozlova, Z.R., and Chernykh, G.G., *J. Chem. Phys*., 2007, vol. 126, p. 214505. https://doi.org/10.1063/1.2734964
53. Rusanov, A.I., *Fazovye ravnovesiya i poverhnostnye yavleniya* (Phase Equilibria and Surface Phenomena), Leningrad: Khimiya, 1967. 388 s.
54. Tolman, R.C., *J. Chem. Phys*., 1949, vol. 17, p. 118.
55. Block, B.J., Das, S.K., Oettel, M., Virnau, P., and Binder, K., *J. Chem. Phys*., 2010, vol. 133, p. 154702. https://doi.org/10.1063/1.3493464
56. Rosales-Pelaez, P., Garcia-Cid, M.I., Valeriani, C., Vega, C., and Sanz, E., *Phys. Rev. (E)*, 2019, vol. 100, no. 2, p. 052609. https://doi.org/10.1103/PhysRevE.100.052609
57. van Gessen, A.E. and Bolhuis, P.G., *J. Chem. Phys*., 2009, vol. 131, p. 164705. https://doi.org/10.1063/1.3253685
58. Baidakov, V.G. and Boltachev, G.Sh., *Phys. Rev. (E)*, 1999, vol. 59, no. 1, p. 469. https://doi.org/10.1103/PhysRevE.59.469
59. Baidakov, V.G., Protsenko, S.P., and Gorbatovskaya, G.G., *Colloid. J*., 2009, vol. 71, no. 4, p. 437. https://doi.org/10.1134/S1061933X09040012
60. Cahn, J.W. and Hilliard, J.E., *J. Chem. Phys*., 1959, vol. 31, no. 3, p. 688.
61. Dias Leines, G., Drautz, R., and Rogal, J., *J. Chem. Phys*., 2017, vol. 146, p. 154702. https://doi.org/10.1063/1.4980082
62. Baidakov, V.G. and Protsenko, K.R., *Colloid. J*., 2019, vol. 81, no. 6, p. 634. https://doi.org/10.1134/S1061933X19060036
63. Rusanov, A.I., *Termodinamisheskie osnovy mekhanokhimii* (Thermodynamic Foundations of Mechanochemistry), St. Petersburg: Nauka, 2006
64. Rusanov, A.I., Tatyanenko, D.V., and Shchekin, A.K., *Colloid. J*., 2010, vol. 72, no. 5, p. 673. https://doi.org/10.1134/S1061933X10050145

65. Baidakov, V.G., Protsenko, S.P., and Tipeev, A.O., *J. Chem. Phys*., 2013, vol. 139, p. 224703. https://doi.org/10.1063/1.4837695
66. Baidakov, V.G. and Protsenko, K.R., *J. Phys. Chem*. (B), 2019, vol. 123, no. 38, p. 8103. https://doi.org/10.1021/acs.jpcb.9b06618
67. Gunawardana, K. and Ceriotti, M., *J. Chem. Phys*., 2018, vol. 148, p. , 204506. https://doi.org/10.1063/1.5021944
68. Cheng, B. and Ceriotti, M., *J. Chem. Phys*., 2018, vol. 148, p. 231102. https://doi.org/10.1063/1.5038396
69. Baidakov, V.G., Rozanov, E.O., and Protsenko, S.P., *Russ. J. Phys. Chem. (A)*, 2021, vol. 95, no. 2, p. 403. https://doi.org/10.1134/S0036024421020059
70. Trudu, F., Donadio, D., and Parrinello, M., *Phys. Rev. Lett*., 2006, vol. 97, p. 105701. https://doi.org/10.1103/PhysRevLett.97.105701
71. Baidakov, V.G. and Tipeev, A.O., *J. Chem. Phys*., 2012, vol. 136, p. 074510. https://doi.org/10.1063/1.3678214
72. Tipeev, A.O., Zanotto, E.D., and Rino, J.P., *J. Phys. Chem. (C)*, 2018, vol. 122, no. 50, p. 28884. https://doi.org/10.1021/acs.jpcc.8b10637
73. Turnbull, T. and Fisher, J.C., *J. Chem. Phys*., 1949, vol. 17, no. 1, p. 71.
74. Sneddon, I.N., *Proc. Roy. Soc. (A)*, 1946, vol. 187, p. 229.
75. Lifshic, I.M. and Gulida, L.S., *Dokl. Akad. Nauk SSSR*, 1952, vol. 87, p. 377.
76. Brener, E.A. and Marchenko, V.I., *Pis'ma Zh. Eksp. Tekh. Fiz*., 1992, vol. 56, p. 381.
77. Hill, R., Proc. Phys. Soc. (A), 1952, vol. 65, p. 349.
78. Kelchner, C.L., Plimpton, S.J., Hamilton, J.C., *Phys. Rev. (B)*, 1998, vol. 58, no. 17, p. 11085. https://doi.org/10.1103/PhysRevB.58.11085
79. Baidakov, V.G. and Tipeev, A.O., *Teplofiz. Vys. Temp*., 2018, vol. 56, no. 2, p. 193.
80. Baidakov, V.G. and Protsenko, S.P., *Mol. Simulation*., 2020, vol. 46, no. 17, p. 1417. https://doi.org/10.1080/08927022.2020.1836371
81. Baidakov, V.G., Protsenko, S.P., and Tipeev, A.O., *JETP Lett*., 2014, vol. 98, no. 12, p. 801. https://doi.org/10.1134/S0021364013250036
82. Levanyuk, A.P., *Zh. Eksp. Tekh. Fiz*, 1974, vol. 66, no. 6, p. 2255.
83. Ashitkov, S.I., Komarov, P.S., Agranat, M.B., Kanel, G.I., and Fortov, V.E., *JETP Lett*., 2014, vol. 98, no. 7, p. 384. https://doi.org/10.1134/S0021364013200022
84. Baidakov, V.G., Tipeev, A.O., and Protsenko, K.R., *Chem. Phys. Lett*., 2017, vol. 680, p. 10. https://doi.org/10.1016/j.cplett.2017.05.014